PNAS RESEARCH ARTICLE | MEDICAL SCIENCES

ADARp110 promotes hepatocellular carcinoma progression via stabilization of CD24 mRNA

Liangzhan Sun[a,b,c,d,e,1], Pengchao Hu[a,f,1], Hui Yang[a], Jun Ren[a], Rong Hu[a], Shasha Wu[a], Yanchen Wang[g], Yuyang Du[a], Jingyi Zheng[g], Fenfen Wang[a], Han Gao[a], Jingsong Yan[a], Yun-Fei Yuan[h], Xin-Yuan Guan[b,c], Jia Xiao[i,2], and Yan Li[g,2]

Affiliations are included on p. 12.

Edited by Douglas Hanahan, Swiss Federal Institute of Technology Lausanne, Lausanne, Switzerland; received May 19, 2024; accepted December 10, 2024

ADAR is highly expressed and correlated with poor prognosis in hepatocellular carcinoma (HCC), yet the role of its constitutive isoform ADARp110 in tumorigenesis remains elusive. We investigated the role of ADARp110 in HCC and underlying mechanisms using clinical samples, a hepatocyte-specific *Adarp110* knock-in mouse model, and engineered cell lines. ADARp110 is overexpressed and associated with poor survival in both human and mouse HCC. It creates an immunosuppressive microenvironment by inhibiting total immune cells, particularly cytotoxic GZMB$^+$CD8$^+$ T cells infiltration, while augmenting Treg cells, MDSCs, and exhausted CD8$^+$ T cells ratios. Mechanistically, ADARp110 interacts with SNRPD3 and RNPS1 to stabilize CD24 mRNA by inhibiting STAU1-mediated mRNA decay. CD24 protects HCC cells from two indispensable mechanisms: macrophage phagocytosis and oxidative stress. Genetic knockdown or monoclonal antibody treatment of CD24 inhibits ADARp110-overexpressing tumor growth. Our findings unveil different mechanisms for ADARp110 modulation of tumor immune microenvironment and identify CD24 as a promising therapeutic target for HCCs.

ADARp110 | hepatocellular carcinoma | macrophage | phagocytosis | CD24

Hepatocellular carcinoma (HCC) is one of the most frequently diagnosed malignancies, accounting for 830,180 deaths around the world in 2020 (1). Regardless of the encouraging results demonstrated by both antiangiogenic therapy and anti-PDL1/PD1 immunotherapy, only a fraction of HCC patients respond favorably, with the majority unable to achieve durable clinical benefits (2, 3). This underscores the urgent need to unravel the mechanisms underlying HCC development and progression and identify effective therapeutic targets.

Recently, the comprehensive analysis of large RNA-seq datasets revealed a trend of increased overall adenosine-to-inosine editing (A-to-I editing) and the expression of adenosine deaminase acting on RNA (ADAR), the enzyme responsible for this editing, in diverse malignancies including HCC (4). Accumulating evidence implicates ADAR in cancer pathogenesis. Prior investigations have focused on identifying the dysregulated editing targets of ADAR in cancers, editing which has been proven to affect mRNA codon readout, splicing, secondary structure, stability, translation efficiency, and the biogenesis and function of noncoding RNA (4–6). Notably, we have previously reported that ADAR fuels HCC onset through editing AZIN1 at residue 367 (7). Additionally, dysregulated editing of CDK13 in thyroid cancer, GLI1 in myeloma, and GABRA3 in breast cancer all exert a significant impact on cancer progression (8–10). Besides the aforementioned RNA editing function, ADAR also exerts tumor-promoting effects independently of RNA editing. For instance, ADAR has been found to drive glioblastoma progression by binding and stabilizing CDK2 mRNA through its dsRNA binding activity (11). In HCC, ADAR facilitates tumor progression by promoting the maturation of miR-27a via interaction with Dicer, acting as a scaffold independent of its RNA editing and dsRNA binding functions (12).

ADAR exists in two isoforms: the constitutively expressed ADARp110 and the interferon-inducible ADARp150. Both isoforms have a double-stranded RNA binding domain (dsRBD) and a deaminase domain, where ADARp150 exclusively contains a Zalpha domain that binds left-handed Z-DNA and Z-RNA, along with a nuclear export signal (NES) (13, 14). In recent years, the significance of interferon-inducible ADARp150, in the tumor immune microenvironment has gained prominence. ADARp150 can bind with double-stranded RNA to down-regulate MDA5/MAVS activation-induced tumor-intrinsic interferon (IFN) responses, thus easing the evasion of tumor cells from immune attack (15, 16). The ablation of ADAR reinstates the sensitivity of tumor cells to IFNs and alleviates PD-1 antibody treatment resistance (17). On the other hand, the functions of constitutively

Significance

This study demonstrates a unique role for ADARp110 in regulating the innate immune response. ADARp110 enhances the "don't eat me" signal by stabilizing CD24 mRNA through the inhibition of STAU1-mediated decay. CD24 overexpression promotes HCC progression by creating an immunosuppressive microenvironment, protecting HCC cells from macrophage phagocytosis, and enhancing cancer cell survival by reducing oxidative stress. Compared to PD-L1, CD24 is more highly expressed and almost exclusively found in liver cancer cells. We demonstrated that targeting CD24 effectively suppresses tumor growth in ADARp110-driven HCC. Notably, treatment with an anti-CD24 monoclonal antibody alone, without combining it with a PD-L1 antibody, effectively inhibits the progression of ADARp110-overexpressing HCC. Our findings identify CD24 as a promising therapeutic target in ADARp110-overexpressing HCC.

Author contributions: L.S., P.H., Y.-F.Y., X.-Y.G., J.X., and Y.L. designed research; L.S., P.H., H.Y., R.H., S.W., Y.W., Y.D., J.Z., F.W., and H.G. performed research; L.S., P.H., J.R., J.Y., and Y.L. analyzed data; and L.S., J.X., and Y.L. wrote the paper.

The authors declare no competing interest.

This article is a PNAS Direct Submission.

[1]L.S. and P.H. contributed equally to this work.

[2]To whom correspondence may be addressed. Email: edwinsiu@connect.hku.hk or liyan181@smu.edu.cn.

This article contains supporting information online at https://www.pnas.org/lookup/suppl/doi:10.1073/pnas.2409724122/-/DCSupplemental.

Published January 14, 2025.

expressed ADAR1p110, typically expressed at substantially higher levels than ADAR1p150 (7), are predominantly uncharacterized. The influence of ADARp110 upregulation on the cancerous immune milieu remains largely ambiguous.

In the present study, we focused on the role of the ADARp110 isoform in HCC. Our findings revealed that hepatocyte-specific *Adarp110* knock-in promoted HCC progression in mouse models. ADARp110 contributes to an immunosuppressive tumor microenvironment by stabilizing CD24 expression, thereby barring macrophage phagocytosis. Additionally, beyond its role in impeding macrophage phagocytosis, CD24 aided HCC cancer cell survival by alleviating oxidative stress. Notably, CD24 expression levels surpassed those of PD-L1 and were almost exclusively expressed in cancer cells in HCC. The application of anti-CD24 monoclonal antibody (mAb) alone was observed to inhibit tumor growth effectively. Collectively, our results suggest that CD24 represents a promising therapeutic target for HCC patients with high ADARp110 expression.

Results

ADARp110 Promotes HCC Progression. Utilizing data from The Cancer Genome Atlas Liver Hepatocellular Carcinoma (TCGA-LIHC) dataset (18), we observed a notable overexpression of ADAR in 34% of HCC patients, with a marked elevation in tumors compared to nontumor tissues (Fig. 1 *A* and *B*). This observation aligns with our clinical cohort results and previously published clinical data (Fig. 1*C* and *SI Appendix*, Fig. S1 *A* and *B*) (19, 20). We further examined the expression of ADARp110 and ADARp150, uncovering that both ADARp110 and ADARp150 were overexpressed in tumor tissues (Fig. 1*D* and *SI Appendix*, Fig. S1*C*). Nevertheless, the change magnitude of ADARp110 was more considerable (2.21-fold vs 1.63-fold) and statistically more significant ($P < 0.0001$ vs $P = 0.011$) than ADARp150. Like ADAR, patients exhibiting higher ADARp110 expression had poorer overall survival rates (Fig. 1*E* and *SI Appendix*, Fig. S1*D*). However, even when applying the Cox proportional hazards model to determine the optimal cutoff point for distinguishing survival curves, the expression level of ADARp150 did not demonstrate prognostic value (*SI Appendix*, Fig. S1*E*). Furthermore, by analyzing liver cancer data from the TCGA and normal liver tissue data from the GTEX database, we confirmed ADARp110 as the predominantly expressed ADAR isoform in both normal and cancerous liver tissues (*SI Appendix*, Fig. S1*F*).

To elucidate the role of ADARp110 in HCC, we developed a genetically modified mouse model, in which hepatocyte-specific *Adarp110* knock-in activated its expression via albumin(Alb)-mediated Cre recombination (*SI Appendix*, Fig. S1 *G–I*). The livers of *Adarp110* transgenic mice appeared unaffected compared to control mice, with no discernible differences in gross liver appearance, liver/body weight ratio, or histologically assessed hepatic architecture (*SI Appendix*, Fig. S1 *J–L*). This suggests that *Adarp110* overexpression alone is insufficient to initiate tumorigenesis in the liver. We further explored the influence of Adarp110 on tumor progression by cross-breeding *Adarp110* knock-in mice and *c-Myc* mice to generate transgenic mice that coexpressed *c-Myc* and *Adarp110* in hepatocytes (*SI Appendix*, Fig. S1 *G–I*) (21). Both WT and *Adarp110*-overexpressed mice developed multifocal liver cancers, but the latter group had noticeably more tumors (average tumor numbers: WT 16.38 *VS Adarp110* 26.88), particularly the larger ones (>0.5 cm) (average tumor numbers: WT 3.8 *VS Adarp110* 6) (Fig. 1 *F* and *G* and *SI Appendix*, Fig. S1*M*). As expected, the survival rate and survival time of *Adarp110*-overexpressed mice were significantly lower than those of the WT group (mean survival days: WT 111 *VS Adarp110* 91) (Fig. 1 *H* and *I*). The above findings indicate that ADARp110 overexpression in HCC correlates with poor survival in both human patients and mice.

ADARp110 Reshapes the Immune Microenvironment in HCC. To discern the means through which ADARp110 expedites HCC progression, we initially generated an *Adarp110* overexpressed murine isogenic hepatoma cell line using lentivirus to probe whether its overexpression promotes HCC progression (*SI Appendix*, Fig. S2 *A* and *B*). Consistent with the previous spontaneous HCC model, the subcutaneous tumor model also demonstrated a significant increase in tumor volume and weight in the *Adarp110* overexpression group (Fig. 2 *A–C*). Notably, differences were not observed in the in vitro clone formation and cell proliferation (Fig. 2 *D* and *E* and *SI Appendix*, Fig. S2*C*), suggesting that the primary function of *Adarp110* might be mediated through modulation of the in vivo tumor microenvironment. Next, we evaluated the immune cell composition in WT and *Adarp110* knock-in tumors via multicolor flow cytometry. Flow cytometry results revealed that compared with WT, *Adarp110* suppressed the infiltration of immune cells ($DAPI^-CD45^+$) (Fig. 2 *F–H* and *SI Appendix*, Fig. S3*A*). Moreover, *Adarp110* knock-in tumors exhibited greater infiltration by Treg cells ($CD4^+CD25^+FOXP3^+$) (Fig. 2*I* and *SI Appendix*, Fig. S3 *B* and *D*) and myeloid-derived suppressor cells (MDSCs) ($CD45^+CD11b^+LY6C^{low}LY6G^{high}$ and $CD45^+CD11b^+LY6G^{low}LY6C^{high}$) (Fig. 2*J* and *SI Appendix*, Fig. S3 *A*, *E*, and *F*). Simultaneously, cytotoxic T cells showed significantly reduced expression of GZMB (Fig. 2*K* and *SI Appendix*, Fig. S3 *B* and *G*) and up-regulated markers associated with exhaustion, namely PD1, TIGIT, and LAG3 (Fig. 2*L* and *SI Appendix*, Fig. S3 *C* and *H–J*) in *Adarp110* knock-in tumors. Further, when we analyzed TCGA-LIHC data using TIMER2.0, we found a positive correlation between ADAR expression and MDSCs and Tregs infiltration, consistent with our mouse model results (Fig. 2*M*). Collectively, these observations suggest that *Adarp110* inhibits immune cell infiltration and establishes an immune suppressive microenvironment in HCC. The discrepancy in tumor immune-microenvironment composition may likely account for the different progression rates between WT and *Adarp110* knock-in models.

The Expression of CD24 Is Elevated in the Adarp110 Knock-in Group. To comprehend the influence of the ADARp110 isoform on the immune environment in HCC, we interrogated mRNA-seq data derived from murine model tumors (Fig. 3*A*). Pathway enrichment analysis revealed significant alterations in cell–cell adhesion and leukocyte migration involved in inflammatory responses (Fig. 3*B*). Within the differently expressed genes linked to these two pathways, a pronounced upregulation of *Cd24a* (termed CD24 in humans) was observed (Fig. 3*A*). A recent study pointed CD24 as an innate immune checkpoint in ovarian and triple-negative breast cancers (22). To disentangle whether the observed upregulation of *Cd24a* mRNA was directly driven by Adarp*110* or is a secondary effect of the tumor microenvironment modulated by *Adarp110*, we further validated CD24 (*Cd24a*) expression in both murine (Hepa1-6) and human (PLC8024 and HepG2) HCC cell lines. CD24 mRNA expression was significantly up-regulated in ADARp110 overexpressed cell lines and down-regulated after ADAR knockdown (Fig. 3*C* and *SI Appendix*, Fig. S4 *A–C*). Correspondingly, flow cytometry analysis demonstrated an upsurge in CD24 protein levels in ADARp110 overexpressed cell lines, decreasing after ADAR suppression (Fig. 3*D*). The immunohistochemistry results further confirmed that CD24 expression is elevated in ADARp110 overexpressing cancer cells (*SI Appendix*, Fig. S4*D*). Furtherly, RNA-seq analysis of the

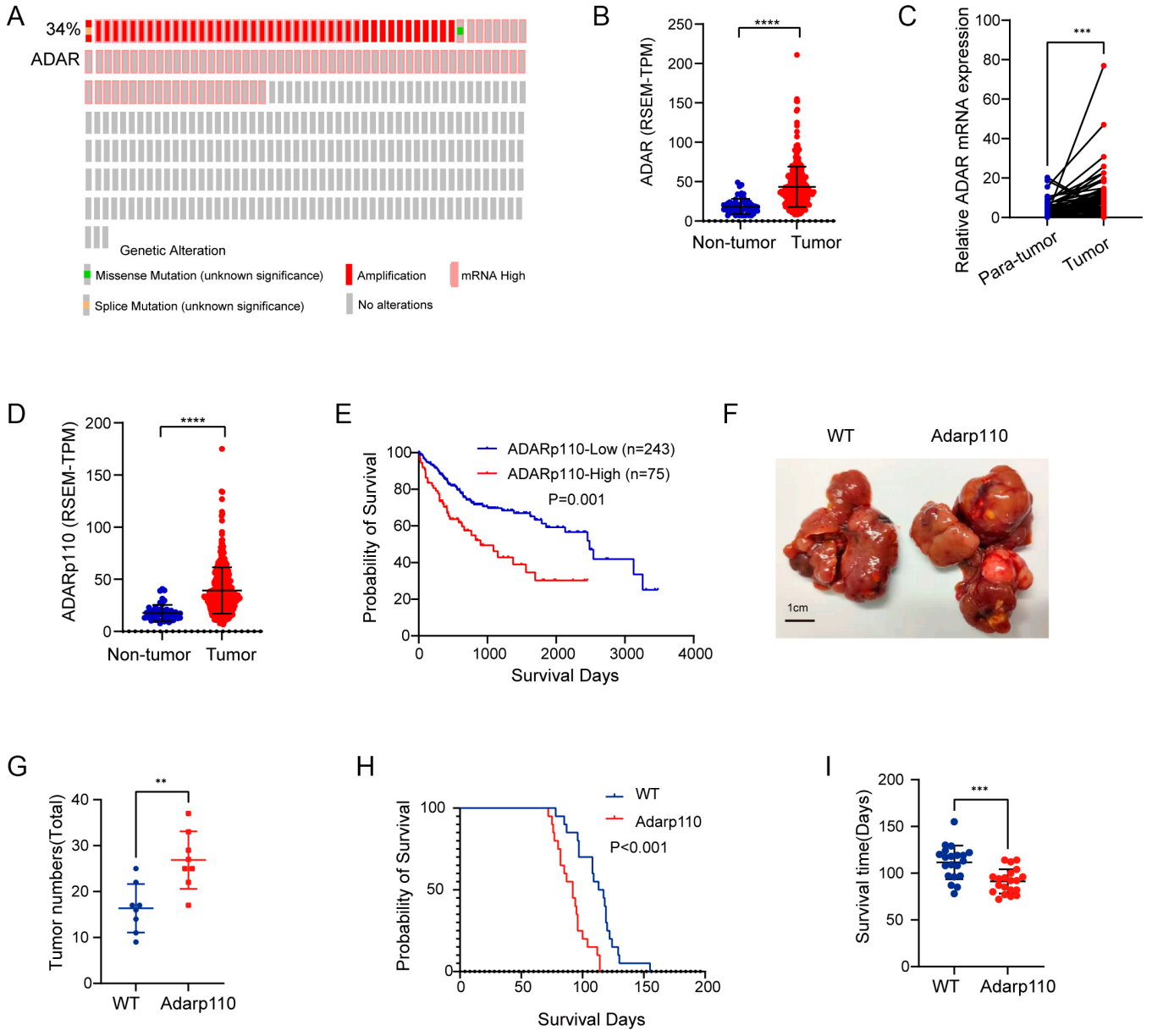

Fig. 1. Overexpression of ADARp110 is associated with poor prognosis in HCC. (*A*) Genetic alterations in the ADAR gene across liver cancer samples from the TCGA-LIHC dataset. Red: amplification; pink: mRNA high; green: missense mutation; orange: splice mutation; gray: no alterations. n = 369. (*B*) Violin plot comparing the mRNA expression levels of ADAR between nontumor (n = 50) and tumor (n = 369) tissues in the TCGA-LIHC dataset. (*C*) Violin plot comparing the relative mRNA expression levels of ADAR between paratumor (n = 69) and paired tumor (n = 69) tissues in our clinical samples. Paratumor: collected from the same patients and histologically confirmed as nontumor tissue. *P*-values were computed using the paired Student's *t* test. (*D*) Violin plot comparing the mRNA expression levels of ADARp110 between nontumor (n = 50) and tumor (n = 369) tissues in the TCGA-LIHC dataset. (*E*) Kaplan–Meier survival curve showing overall survival in patients with high (n = 75) versus low (n = 243) ADARp110 expression. *P*-values were computed using the log-rank test. (*F* and *G*) Representative images (*F*) and quantification of tumor numbers (*G*) of c-Myc-driven WT and Adarp110 hepatocyte-specific knock-in mouse models of HCC (n = 8). (Scale bar, 1 cm.) (*H*) Kaplan–Meier survival curve indicating overall survival of WT and Adarp110 hepatocyte-specific knock-in mouse from mice HCC model (n = 20). *P*-values were computed using the log-rank test. (*I*) Violin plot comparing the survival days of WT and Adarp110 hepatocyte-specific knock-in mouse from mice HCC model (n = 20). Data are presented as mean ± SD. *P*-values were computed using the unpaired Student's *t* test (*B*, *D*, *G*, and *I*). ***$P < 0.001$, ****$P < 0.0001$.

human HCC cell line HepG2 also showed a marked upregulation of CD24 in the ADARp110 overexpressed group (Fig. 3*E*). In concordance with the murine data, cell–cell adhesion and immune system-related processes were among the enriched pathways in these HepG2 cells (Fig. 3*F*).

To further validate these findings in a clinical context, we analyzed data from in-house clinical samples, TCGA and GSE14520 (18, 23). CD24 was indeed highly expressed in the tumors (*SI Appendix*, Fig. S4 *E–G*), and positively correlated with ADAR (*SI Appendix*, Fig. S4 *H–J*). Interestingly, ADARp110 exhibited a stronger correlation with CD24 compared to ADARp150, as evidenced by a higher R-value and a lower *P*-value (Fig. 3 *G* and *H*). To exclude the possibility that the observed correlation between ADARp150 and CD24 expression in the TCGA-LIHC dataset was attributable to the alternative translation of ADARp110 protein from ADARp150 transcript (24), we overexpressed a mutant form of ADARp150 (ADARp150-Mut, p150 GCG mut) in the human HCC cell lines PLC8024 and HepG2 (*SI Appendix*, Fig. S4*K*). This mutation altered the second start codon ATG (ATG to GCG), thereby ensuring that only the full-length p150 isoform was produced (11). Notably, overexpression of ADARp150-Mut did not increase CD24 expression (Fig. 3*I*). Additionally, in a mouse Hepa1-6 cell line, overexpression of wild-type Adarp150 also failed to elevate CD24 (*Cd24a*) expression (Fig. 3*I* and *SI Appendix*,

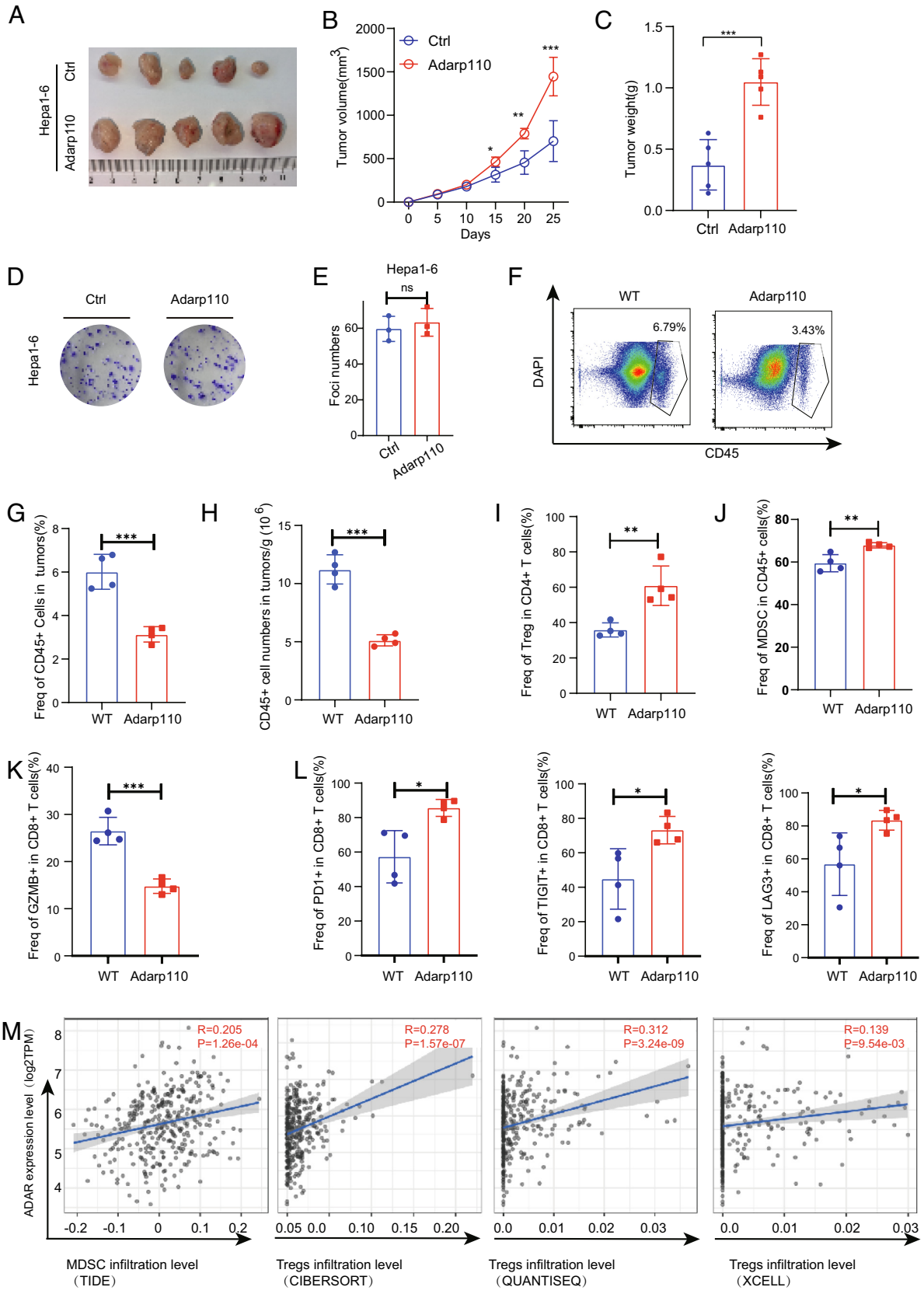

Fig. 2. ADARp110 generates an immune-suppressive microenvironment in HCC. (*A–C*) Representative image of tumor formation (*A*), tumor volume over time (*B*), and tumor weights (*C*) at the experimental endpoint in the Hepa1-6 subcutaneous model (n = 5). (*D* and *E*) Representative images (*D*) and quantification of foci formation (*E*) induced by the indicated cells (n = 3). (*F–H*) Total immune cells ($CD45^+$) infiltration measured by flow cytometry. Representative images (*F*), statistical results of the infiltration ratio (*G*), and number of infiltrating immune cells per gram of tissue (*H*) in WT and *Adarp110*-overexpressing tumors (n = 4). (*I–L*) Statistical results of indicated immune cells in WT and *Adarp110*-overexpressing tumors analyzed by flow cytometry (n = 4). (*M*) Scatter plot showing the correlation between ADAR expression and the infiltration of MDSCs and Tregs in human HCC, analyzed using the TIMER2.0 platform through indicated computational tools, including CIBERSORT, QUANTISEQ, and XCELL. The *P*-value was calculated using Pearson's correlation coefficient. Data are presented as mean ± SD. *P*-values were computed using the unpaired Student's *t* test (*B*, *C*, *E*, and *G–L*). *$P < 0.05$, **$P < 0.01$, ***$P < 0.001$, ns: not significant.

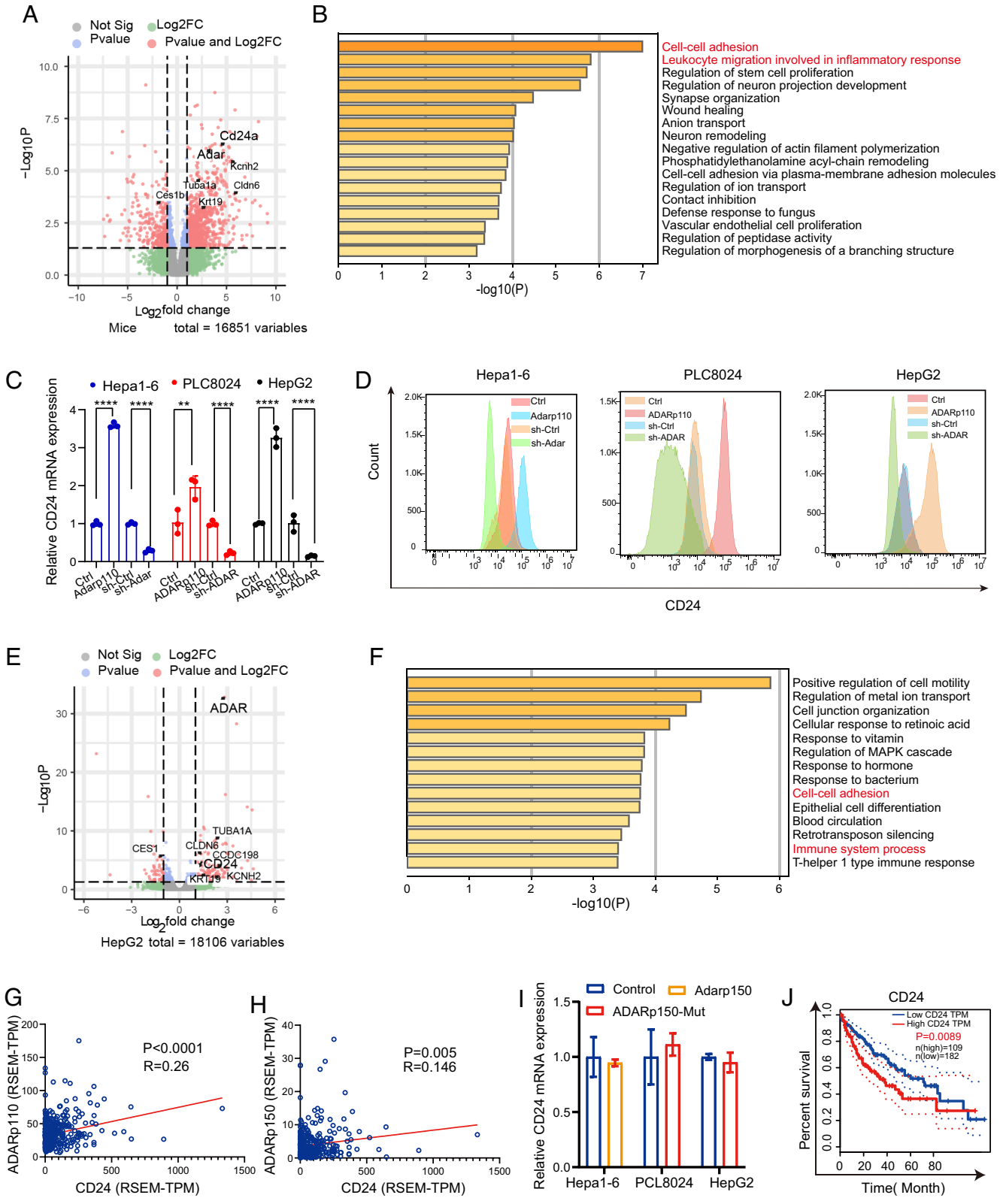

Fig. 3. ADARp110 regulates CD24 expression in HCC cells. (*A*) Volcano plot showing the differential expression of genes between WT and *Adarp110* knock-in mouse models of HCC. (*B*) Gene Ontology (GO) enrichment analysis highlighting the biological processes that are significantly enriched in the RNA-seq data comparing *Adarp110* knock-in and wild-type (WT) mouse models of HCC. The significance of each process is represented by −log10(P). (*C* and *D*) The expression of CD24 in indicated cells was verified by qPCR (*C*) and flow cytometry (*D*) (n = 3). (*E*) Volcano plot showing the differential expression of genes between control and ADARp110 overexpressed human HCC HepG2 cells. (*F*) Gene Ontology (GO) enrichment analysis highlighting the biological processes that are significantly enriched in the RNA-seq data comparing control and ADAR110 overexpressed human HCC HepG2 cells. The significance of each process is represented by −log10(P). (*G* and *H*) Scatter plots showing the correlation between CD24 and ADARp110 (*G*) and ADARp150 (*H*) expression, based on data from the TCGA-LIHC dataset. *P*-values were calculated using Pearson's correlation coefficient. (*I*) qPCR was performed to assess CD24 mRNA expression levels in indicated cells after overexpression of ADARp150 (yellow bars), ADARp150-Mut (red bars), or control (blue bars) (n = 3). (*J*) Kaplan–Meier survival curve comparing overall survival in patients with high (n = 109) versus low (n = 182) CD24 expression, as determined by the log-rank test (*P* = 0.0089). Data are presented as mean ± SD. *P*-values were computed using the unpaired Student's *t* test (*C* and *I*). $^{**}P < 0.01$, $^{***}P < 0.001$.

Fig. S4*K*). Moreover, consistent with the ADARp110 results, CD24 overexpression was associated with poor overall survival and high recurrence rates in HCC (Fig. 3*J* and *SI Appendix*, Fig. S4 *L* and *M*). Together, the above findings compellingly demonstrated that ADARp110 significantly influences the expression of CD24 in HCC.

ADARp110 Modulates an Immunosuppressive Microenvironment via Upregulation of CD24. To investigate the role of CD24 in the ADARp110-induced immunosuppressive tumor microenvironment and HCC progression, we utilized pHrodo Red to stain tumor cells isolated from primary mouse tumors and cocultivated them with bone marrow–derived macrophages (BMDMs). *Adarp110* knock-in significantly inhibited phagocytic clearance by BMDMs (Fig. 4 *A* and *B*). Consistent results were observed in our established cell lines, and this effect was abrogated following *Cd24* knockdown (Fig. 4*C* and *SI Appendix*, Fig. S5 *A* and *B*). To assess the role of CD24 in orchestrating the immune microenvironment in ADARp110 overexpressing HCC, we generated a subcutaneous tumor model in immune-competent mice using *Adarp110* overexpressed Hepa1-6 cell line. Knocking down *Cd24a* significantly inhibited tumor growth, as evidenced by reduced tumor volume and weight (Fig. 4*D*). However, we did not observe a significant inhibitory effect from tumors lacking *Adarp110* expression in combination with sh-*Cd24a* in this model. This may be related to the reduced expression levels of *Cd24a* after the knockdown of *Adar* (*SI Appendix*, Fig. S5 *C–E*).

Specifically, flow cytometry analysis revealed that *Cd24a* knockdown in *Adarp110* overexpressed tumor inflamed the tumor environment by amplifying immune cell infiltration (Fig. 4 *E–G*) and reducing MDSCs as well as Tregs proportion (Fig. 4 *H* and *I*). It also enhanced GZMB expression and decreased immune checkpoint proteins PD1, TIGIT, and LAG3 expression in $CD8^+$ T cells (Fig. 4 *J* and *K*). Intriguingly, tumor-associated macrophages isolated from *CD24a* knockdown tumors exhibited elevated IFNβ, IFNγ, and TNFα expression, indicating a shift toward a more immunostimulatory phenotype (Fig. 4*L*). Considering that IFNβ, IFNγ, and TNFα are potent inducers of immune cell recruitment (25), and our bulk-seq data suggested a link between ADARp110 and immune cell migration (Fig. 3 *B* and *F*), we conducted a $CD4^+$ T/$CD8^+$ T cell migration assay to further investigate the effect of ADARp110/CD24 expression in tumor cells on T cells recruitment. After coculturing tumor cells and BMDMs for 24 h, $CD4^+$ T cells or $CD8^+$ T cells were seeded in the upper chambers and induced to migrate (*SI Appendix*, Fig. S5*F*). Our results revealed that the ADARp110 overexpression group demonstrated the weakest ability to recruit $CD4^+$ and $CD8^+$ T cells (*SI Appendix*, Fig. S5 *G* and *H*). However, upon CD24 knockdown in the WT/ADARp110 groups, the recruitment of $CD4^+$ and $CD8^+$ T cells was significantly enhanced, and the differences between the WT and ADARp110 groups were no longer observed (*SI Appendix*, Fig. S5 *G* and *H*), suggesting that the observed inhibition is dependent on CD24 expression. In summary, by up-regulating CD24, ADARp110 overexpressed cancer cells manage to evade macrophages' phagocytic clearance. The knockdown of CD24 ignites the immunostimulatory microenvironment in ADARp110 overexpressed tumors.

CD24 Promotes Oxidative Stress Resistance in HCC. We next elucidated the contribution of the "do not eat me" signal, CD24-Siglec10 (22), in ADARp110-provoked HCC progression by depleting macrophage using clodronate liposome (*SI Appendix*, Fig. S6 *A* and *B*) (26). At the early stage of tumor growth, the clearance of macrophages almost nullified the growth difference between ADARp110 and control groups, corroborating the key role of macrophages in mediating the tumorigenic abilities of ADARp110. Unexpectedly, even after macrophage depletion, the ADARp110 group still formed larger tumors in the late stage, suggesting that besides preventing macrophage phagocytizing, other mechanisms, apart from preventing macrophage phagocytosis, could expedite the progression of ADARp110 overexpressed tumors (Fig. 5 *A–C*). Furthermore, unlike the knockdown of ADAR rendering tumor cells susceptible to IFN treatment, neither ADARp110 overexpression nor CD24 knockdown altered IFN sensitivity (*SI Appendix*, Fig. S6*C*). To explore other possible mechanisms promoting HCC progression, we performed Gene Set Enrichment Analysis (GSEA) using transcriptional data and noticed a marked downregulation of reactivate oxygen species pathway signature concurrent with both ADAR and CD24 expression (Fig. 5*D* and *SI Appendix*, Fig. S6*D*). Moreover, peroxisome and oxidative stress response signatures were also down-regulated with CD24 expression (Fig. 5*D*). Given these findings, we hypothesize that the ADARp110-CD24 pathway could play a role in ameliorating oxidative stress in HCC. To test this hypothesis, we introduced a low-dosage H_2O_2 (50 μM) into the cell medium and assessed cell proliferation and clone formation. ADARp110 promoted HCC cell growth under oxidative stress, but this resistance advantage waned following CD24 knockdown (Fig. 5 *E–G*). Consistently, ADARp110 protected HCC cells from apoptosis when treated with high-dose H_2O_2 (200 μM) in a CD24-dependent manner (Fig. 5 *H* and *I*). These findings underscore the role of CD24 in providing resistance to oxidative stress and hint that this could be another contributing factor to HCC progression.

ADARp110 Stabilizes CD24 mRNA by Inhibiting STAU1-Mediated mRNA Decay. Subsequently, we initiated the exploration of the mechanisms underlying ADARp110's regulation of CD24 expression. ADAR can regulate gene expression either through direct RNA editing, affecting target RNA stability and splicing, or indirectly via modulation of primary micro-RNA processing thus influencing the expression of downstream genes. We found that ADARp110 overexpression increased global editing events, which correspondingly decreased upon ADAR knockdown (Fig. 6*A* and *SI Appendix*, Fig. S7*A*). However, no correlation was found between RNA editing level and global mRNA expression level (Fig. 6*B* and *SI Appendix*, Fig. S7*B*), and no editing sites were detected within the CD24 mRNA. To assess whether ADARp110 indirectly regulates CD24 mRNA expression via micro-RNA, we conducted micro-RNA sequencing using ADARp110 overexpressed and knockdown cell lines to identify ADARp110-regulated micro-RNAs. However, there was no overlap between ADARp110-regulated micro-RNAs and those predicated to target CD24 using miRBD (*SI Appendix*, Fig. S7 *C* and *D*). Thus, we infer ADARp110 regulates CD24 independently from mRNA editing and micro-RNA regulation.

Further exploration outlined how ADARp110 regulates CD24. We utilized the Crispr-cas9 system to generate ADAR knockout cell lines and subsequently reintroduced either wild-type ADARp110, a catalytically inactive mutant (Cat-mut), or an RNA binding domain inactive mutant (RBD-mut). (*SI Appendix*, Fig. S8 *A* and *B*). Both ADARp110 and ADARp110 CA-mut were able to rescue CD24 expression, whereas the RBD-mut failed to show a similar phenotype (Fig. 6*C*). This suggests that the RNA binding activity of ADARp110 is crucial for its regulatory effect on CD24. Further, we applied actinomycin D to inhibit RNA transcription and observed that ADARp110 enhanced the stability of CD24 mRNA (Fig. 6*D* and *SI Appendix*, Fig. S8*C*). These findings indicate that ADARp110 up-regulates CD24 expression by binding to CD24 mRNA and increasing its stability. Published ADAR CLIP-seq data confirmed our results, showcasing ADAR binding motif enrichment in four

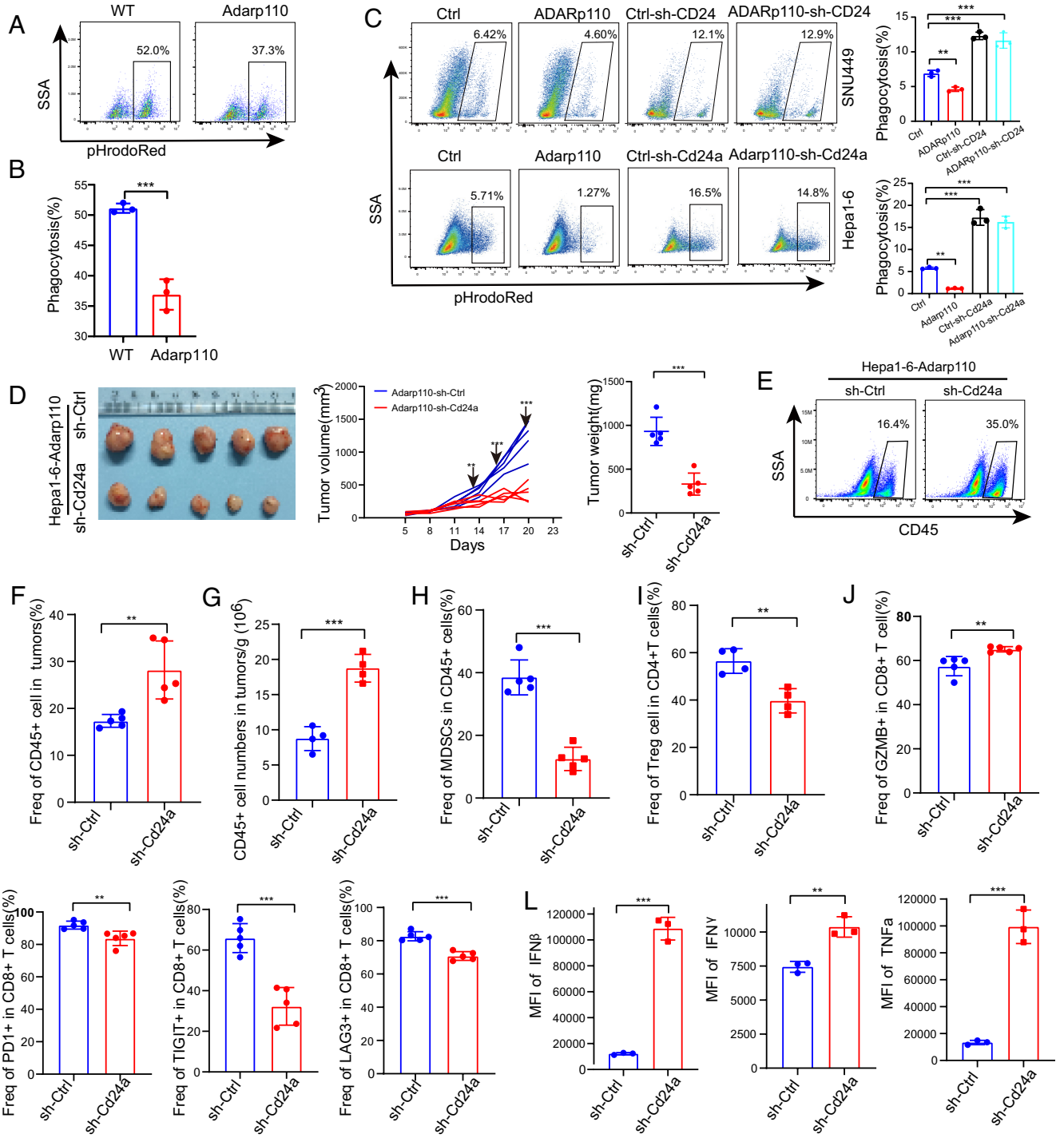

Fig. 4. ADARp110 inhibits macrophage phagocytosis and generates a CD24-dependent immune suppressive microenvironment. (*A* and *B*) Representative flow cytometry plots (*A*) and quantification of phagocytosis (*B*) of pHrodo Red-labeled cancer cells from the primary tumor by BMDMs (n = 3). (*C*) Representative image and quantification of phagocytosis of indicated generated cancer cell lines by BMDMs were measured with flow cytometry (n = 3). (*D*) Representative image of tumor formation (*Left*), tumor volume over time (*Middle*), and tumor weights (*Right*) at the experimental endpoint in the Hepa1-6 *Adarp110* overexpressing subcutaneous model (n = 5). (*E–G*) Total immune cell (CD45+) infiltration measured by flow cytometry. Representative images (*E*), statistical results of the infiltration ratio (*F*), and number of infiltrating immune cells per gram of tissue (*G*) in Ctrl and *Cd24a* knockdown tumors from the Hepa1-6 *Adarp110* overexpression subcutaneous model (n = 5). (*H–K*) Flow cytometry analysis of indicated immune cells in Ctrl and *Cd24a* knockdown tumors from the Hepa1-6 *Adarp110* overexpression subcutaneous model (n = 5). (*L*) Expression levels of IFNβ, IFNγ, and TNFα in TAMs isolated from the indicated subcutaneous tumors, measured by flow cytometry (n = 3). Data are presented as mean ± SD. *P*-values were computed using the unpaired Student's *t* test (*B*, *D*, *F–L*) or one-way ANOVA (*C*). $^{**}P < 0.01$, $^{***}P < 0.001$.

distinct CD24 mRNA regions (Fig. 6*E*) (27). We corroborated this finding by overexpressing ADARp110-3XFlag in ADAR knockout cells and conducting an RNA immunoprecipitation experiment followed by qPCR. All four fragments were confirmed to bind with ADARp110, with fragment 4 located in the 3′-UTR of CD24 showing the highest binding capacity (Fig. 6*F* and *SI Appendix*, Fig. S8*D*).

We progressed to an RNA–protein pull-down assay with the 3′-UTR of CD24 and the resulting protein complex analysis via mass spectrometry. ADARp110, SLC25A3, LMNA, NLE1, MRPL18, SNRPD3, NSUN2, and RNPS1 binding with the 3′-UTR of CD24 were identified in ADARp110 overexpressed cells but not in ADAR knockout cells. In contrast, GAR1, MCM3,

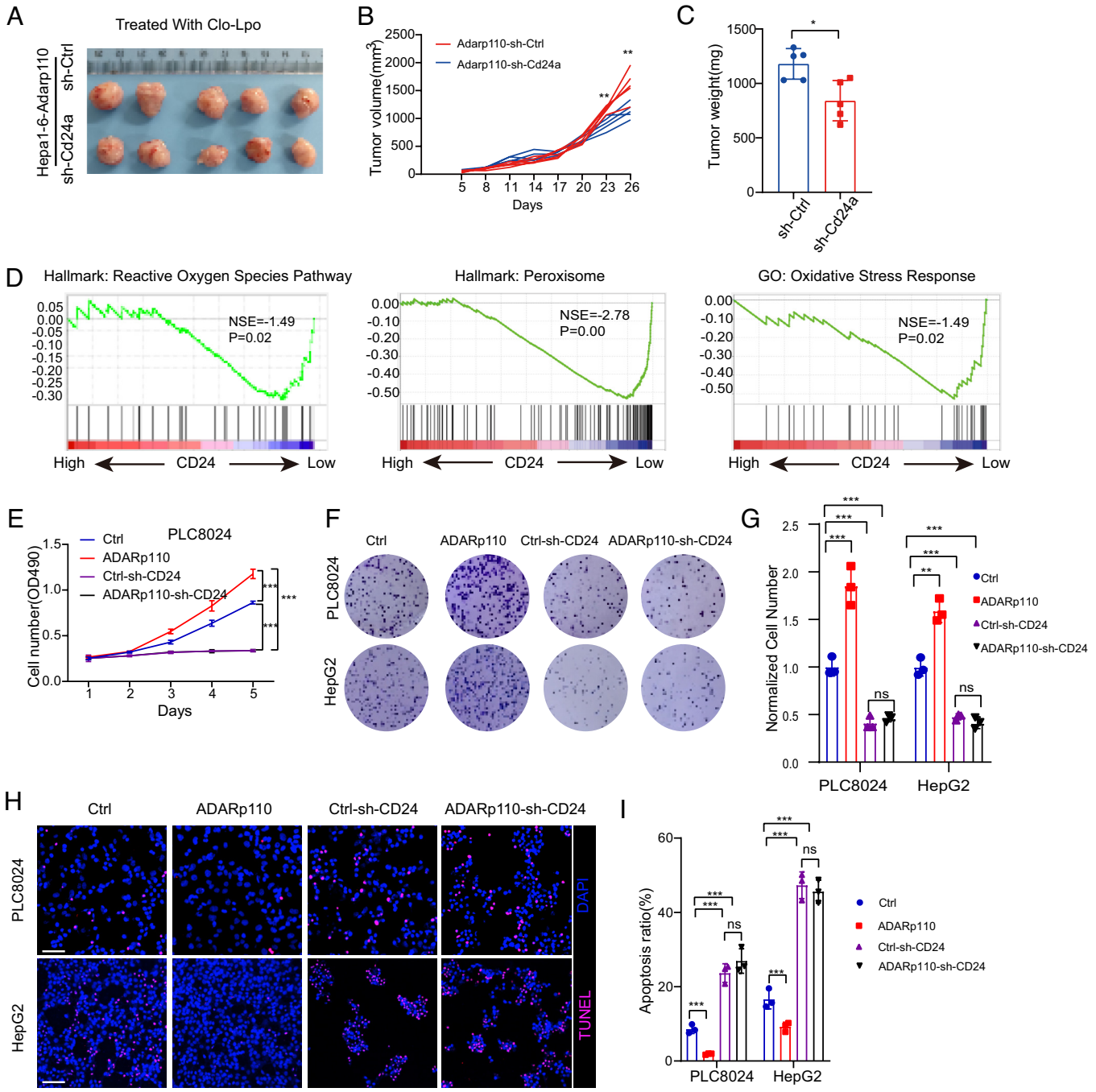

Fig. 5. ADARp110 relieves oxidative stress by up-regulating CD24. (*A–C*) Representative image of tumor formation (*A*), tumor volume over time (*B*), and tumor weights (*C*) at the experimental endpoint after macrophage depletion in the Hepa1-6 Adarp110 overexpressing subcutaneous model (n = 5). (*D*) GSEA comparing gene sets in TCGA-LIHC patients with high versus low CD24 levels. GSEA shows a significant association between CD24 expression and the reactive oxygen species pathway (*Left*), peroxisome (*Middle*), and oxidative stress response (*Right*). (*E*) Cell viability of the indicated cells determined by the XTT assay after 50 μM H_2O_2 treatment over five days (n = 3). (*F* and *G*) Representative images (*F*) and quantification of foci formation (*G*) induced by 1,000 cells per well of the indicated cells after treatment with 50 μM H_2O_2 for seven days (n = 3). (*H* and *I*) Representative images (*H*) and statistical results (*I*) of apoptosis in the indicated cells after treatment with 200 μM H_2O_2 for 48 h, measured by the TUNEL assay (n = 3). Cells were stained with DAPI (blue) to label nuclei and TUNEL (magenta) to detect apoptotic cells. TUNEL-positive cells indicate apoptosis. (Scale bar, 50 μm.) Data are presented as mean ± SD. *P*-values were computed using the unpaired Student's *t* test (*B* and *C*) or one-way ANOVA (*E*, *G*, and *I*). $^{**}P < 0.01$, $^{***}P < 0.001$.

CTTN, and RPL36A were only detected in ADAR knockout cells (Fig. 6*G*). Based on these observations, we postulated that ADARp110, SLC25A3, LMNA, NLE1, MRPL18, SNRPD3, NSUN2, and RNPS1 may contribute to the ADARp110-induced CD24 mRNA stability, while GAR1, MCM3, CTTN, and RPL36A could be involved in its decay.

To test this hypothesis, a siRNA library was designed to target SLC25A3, LMNA, NLE1, MRPL18, SNRPD3, NSUN2, and RNPS1(*SI Appendix*, Fig. S8 *E* and *F*). Inhibiting either SNRPD3 or RNPS1 led to reduced CD24 expression and an associated coimmunoprecipitation experiment confirmed ADARp110's binding with SNRPD3 and RNPS1 (Fig. 6 *H* and *I* and *SI Appendix*, Fig. S8*G*). These results suggest that ADARp110 binds with SNRPD3 and RNPS1 to stabilize CD24 mRNA. Previous studies have reported that ADAR can inhibit STAU1-mediated mRNA decay by competitively binding to the 3'-UTR of target genes. Analyzing the interaction between GAR1, MCM3, CTTN, and RPL36A, which is associated with the 3′-UTR of CD24 in ADAR

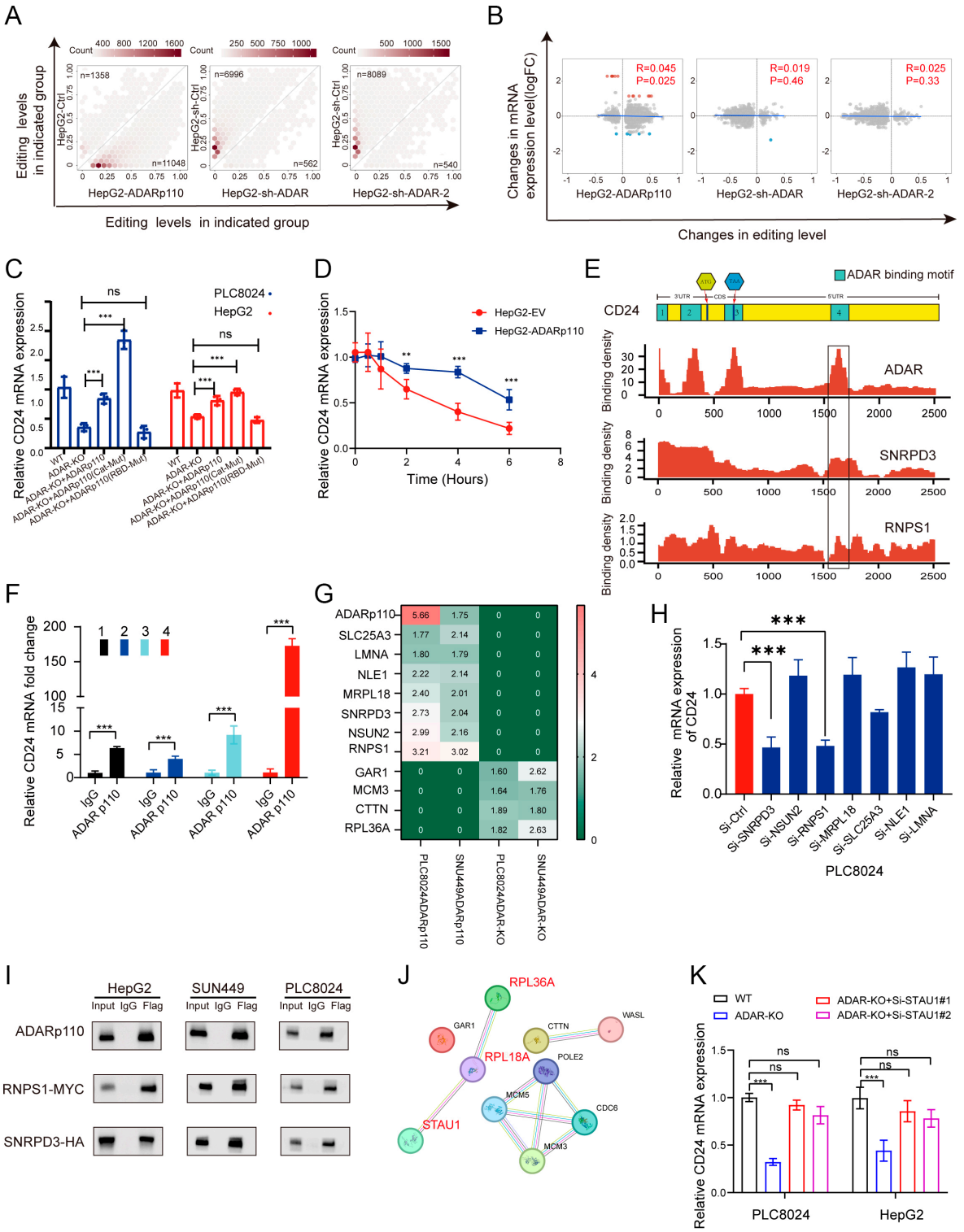

Fig. 6. ADARp110 binds to and stabilizes CD24 mRNA by inhibiting STAU1-mediated mRNA degradation. (*A*) Scatter plots showing the RNA editing levels of HepG2 control cells (HepG2-Ctrl) and HepG2 cells with ADARp110 overexpression (HepG2-ADARp110) or ADAR knockdown (HepG2-sh-ADAR and HepG2-sh-ADAR-2). Each hexagon represents a group of editing sites, with color intensity indicating the number of editing sites. n indicated the total editing events. (*B*) Scatter plots illustrating the relationship between changes in RNA editing levels (x-axis) and corresponding changes in mRNA expression (log fold change, y-axis) in the indicated cells compared to the corresponding controls. (*C*) qPCR was performed to assess relative CD24 mRNA expression levels in indicated cells (n = 3). (*D*) Time-course analysis of CD24 mRNA expression with qPCR after Actinomycin D (5 μg/ml) treatment in HepG2 cells (n = 3). (*E*) Scaled schematic of CD24 mRNA (*Upper*) and the binding sites of the indicated proteins (*Bottom*), X-axis: scaled CD24 mRNA transcript. Y-axis: relative binding affinity of indicated proteins. (*F*) Relative enrichment of CD24 mRNA fragments in ADARp110-RIP compared to IgG in the indicated cells was measured using qPCR (n = 3). (*G*) Heat maps showing the binding capacity of indicated proteins with 3′-UTR of CD24 mRNA. Color scales represent normalized binding scores (n = 3). (*H*) Relative CD24 mRNA expression after knockdown of the indicated gene with siRNA in the PLC8024 cell line (n = 3). (*I*) Immunoprecipitation was conducted using Flag-tagged ADARp110 (Flag) or IgG control antibodies, with cell lysates serving as input controls. Western blotting was used to detect ADARp110-Flag, RNPS1-MYC, and SNRPD3-HA in the immunoprecipitates. (*J*) Protein–protein interaction analysis of proteins binding to the 3′-UTR of CD24 in ADAR knockout cells using STRING. (*K*) Relative CD24 mRNA expression after knockdown of STAU1 with siRNA in the indicated cell line (n = 3). Data are presented as mean ± SD. *P*-values were computed using the unpaired Student's *t* test (*D* and *F*) or One-Way ANOVA (*C*, *H*, and *K*). $^{**}P < 0.01$, $^{***}P < 0.001$.

knockout cells, using STRING (28), revealed RPL36A interaction with RPL18A, a confirmed STAU1 interactor (Fig. 6*J*). To verify whether STAU1 affects ADARp110-medicated CD24 mRNA stability, we silenced STAU1 and observed that this rescued the downregulation of CD24 caused by ADARp110 knockdown (Fig. 6*K* and *SI Appendix*, Fig. S8*H*). In summary, these findings illustrate that ADARp110 interacts with SNRPD3 and RNPS1 to stabilize CD24 mRNA by competitively inhibiting the binding of STAU1 to the 3′-UTR of CD24.

CD24 Is a Promising Therapeutic Target in HCC. Through a comprehensive analysis of TCGA-LIHC data utilizing TIMER2.0, a positive correlation was observed between *CD24* expression and the infiltration of myeloid-derived suppressor cells as well as Tregs in HCC (Fig. 7*A*). An examination of single-cell RNA-seq data (GSE125449) further underscored the highly specific expression pattern of *CD24*, predominantly localized to malignant HCC cells, with minimal expression in plasma cells, $CD8^+$ Tex cells, monocytes, macrophages, fibroblast, and endothelial cells (Fig. 7*B*) (29). Of note, PD-L1 expression was modest and did not vary significantly between tumor and nontumor tissues in HCC. In contrast, CD24 expression was markedly higher than PD-L1 and exhibited elevated expression levels in tumor tissues compared to nontumor tissues (Fig. 7*C*). Those facts make CD24 a specific and promising therapeutic target of HCC. To test this possibility, human HCC cells were treated with anti-CD24 mAb. This intervention alone demonstrated a significant inhibition of tumor cell growth under oxidative stress (Fig. 7 *D* and *E*). To further assess the efficacy of CD24 targeting in vivo, a subcutaneous tumor model was established using the human HCC cell line PLC8024 in NOD-SCID mice. Remarkably, tumor growth driven by ADARp110 overexpression was effectively suppressed following treatment with anti-CD24 mAb alone (Fig. 7*F*). Collectively, these results accentuate CD24 as a promising therapeutic target in ADARp110 overexpressed HCC patients.

Discussion

Until recently, our comprehension of ADAR function in vivo has been predominantly informed by ADAR knockout or conditional knockout mouse models. However, these models are suboptimal for exploring the function and mechanism of ADAR in HCC due to the lethal consequence of ADAR knockout, and liver-specific conditional knockout also results in severe growth retardation and high mortality (30). Herein, we employed a hepatocyte-specific conditional knock-in mouse model to study the function of ADARp110 in HCC. To the best of our understanding, this is the inaugural investigation of ADARp110 function in HCC utilizing a hepatocyte-specific conditional knock-in mouse model.

Historically, the ADARp150 isoform has been discerned as the chief isoform regulating innate immune homeostasis (4). Localized in the cytoplasm, ADARp150 encompasses a Z-DNA/RNA binding domain that facilitates the inhibition of the activation of the MDA5/MAVS, PKR, and ZBP1 pathway (16, 31). Prior research has demonstrated that ADAR knockout in tumor cells can overcome anti-PD-1 resistance by enhancing immune cell infiltration and fostering an inflammatory tumor environment. A congruent outcome was evident in B2m-null tumors, which are unrecognized by $CD8^+$ T cells, suggesting that beyond $CD8^+$ T cells, ADAR-KO modulates additional mechanisms and immune cell types that modulate the tumor immune microenvironment and tumor growth (17, 32). In the present study, we found that ADARp110 contributes to an immunosuppressive microenvironment in HCC by inhibiting immune cell infiltration and increasing the ratio of MDSC, Treg, and exhausted T cells.

Additionally, we found that ADARp110 but not ADARp150 regulates CD24 expression in HCC. CD24 is ubiquitously overexpressed in various cancers and can interact with macrophages via SIGLEC10. The CD24–SIGLEC10 axis has been reported as an innate immune checkpoint in ovarian cancer, triple-negative cancer, and melanoma (22, 33). Corroborating these findings, our data indicate that ADARp110 facilitates HCC cancer cell evasion from macrophage phagotrophy in a CD24-dependent manner. Silencing CD24 in ADARp110 overexpressed HCC rejuvenates the tumor immune microenvironment by bolstering immune cell infiltration and reducing the ratio of MDSC, Treg, and exhausted T cells. Intriguingly, we recorded a substantial decrease in the growth of tumors treated with anti-CD24 antibody in NOD-scid mice, which lacked T, B, and functional NK cells, suggesting that macrophages are key to the benefits of targeting ADARp110. These findings partly elucidate how ADAR knockout overcomes immunotherapy resistance independent of $CD8^+$ T cells.

ADAR's ability to operate as an RNA-binding protein represents a key strategy by which it modulates the transcriptome. ADAR's binding to RNA substrates is instrumental in determining transcript stability and gene expression, facilitated by its interaction with HuR (ELAVL1) (34). Another study reported how ADARp110 translocates to the cytoplasm and competitively restricts STAU1 attachment to the 3′-UTR of various antiapoptotic gene transcripts, thereby inhibiting STAU1-triggered mRNA degradation (35). In our study, we observed that ADARp110 interacts with both RNPS1 and SNRPD3, thereby competitively impeding STAU1's binding to the 3′-UTR of *CD24*. We examined previously published data and observed that CD24 was not listed as an ADAR/STAUF1-regulated gene (16). This inconsistency could be attributed to the context-dependent effects of ADAR1 on gene expression, specifically in A172 glioblastoma cells exposed to UV irradiation. Moreover, the expression level of CD24 in our cell line is significantly higher (7 to 170-fold) compared to the A172 cell line, indicating a distinct expression pattern of CD24 in HCC compared to glioblastoma cells. Notably, direct binding of STAU1 to the 3′-UTR of *CD24* was undetectable in ADAR knockout cells, potentially due to the sudden mRNA decay that may follow STAU1 binding. Separate research revealed that the interaction of Staufen1 with dsRNA is more dynamic, whereas that of ADAR1 is very static (36). However, we did notice the direct binding of RPL36A to the 3′-UTR of *CD24* in ADAR knockout cells. Given previous evidence of RPL36A's interaction with RPL18A, and the latter's with STAU1 (28), we theorize a possible decay mechanism involving these elements. The mRNA destined for decay binds to RPL36A, which subsequently recruits RPL18A and STAU1 to initiate the decay process. The ADARp110/RNPS1/SNRPD3 complex competitively inhibits the binding of RPL36A to RNA substrates. This theory, along with the dynamics of RNA decay, demands further exploration. It is important to note that additional factors, such as methylation, ROS, and hypoxia, may also influence CD24 expression independently of ADARp110 (37–39). This likely explains the relatively low R-value observed in the TCGA-LIHC database.

ADAR is essential for normal tissue homeostasis and the genetic ablation of *Adar* in mice is lethal. Thus, targeting ADAR might entail significant risks. More pragmatic approaches could involve targeting specific downstream effectors of ADARp110 that are implicated in cancer progression. We have demonstrated that CD24, a downstream target of ADARp110, plays a pivotal role in immune evasion and survival under oxidative stress in HCC. Notably, treating ADARp110 highly expressed tumors with an anti-CD24 antibody alone can effectively inhibit tumor growth. This observation aligns with previous research showing a

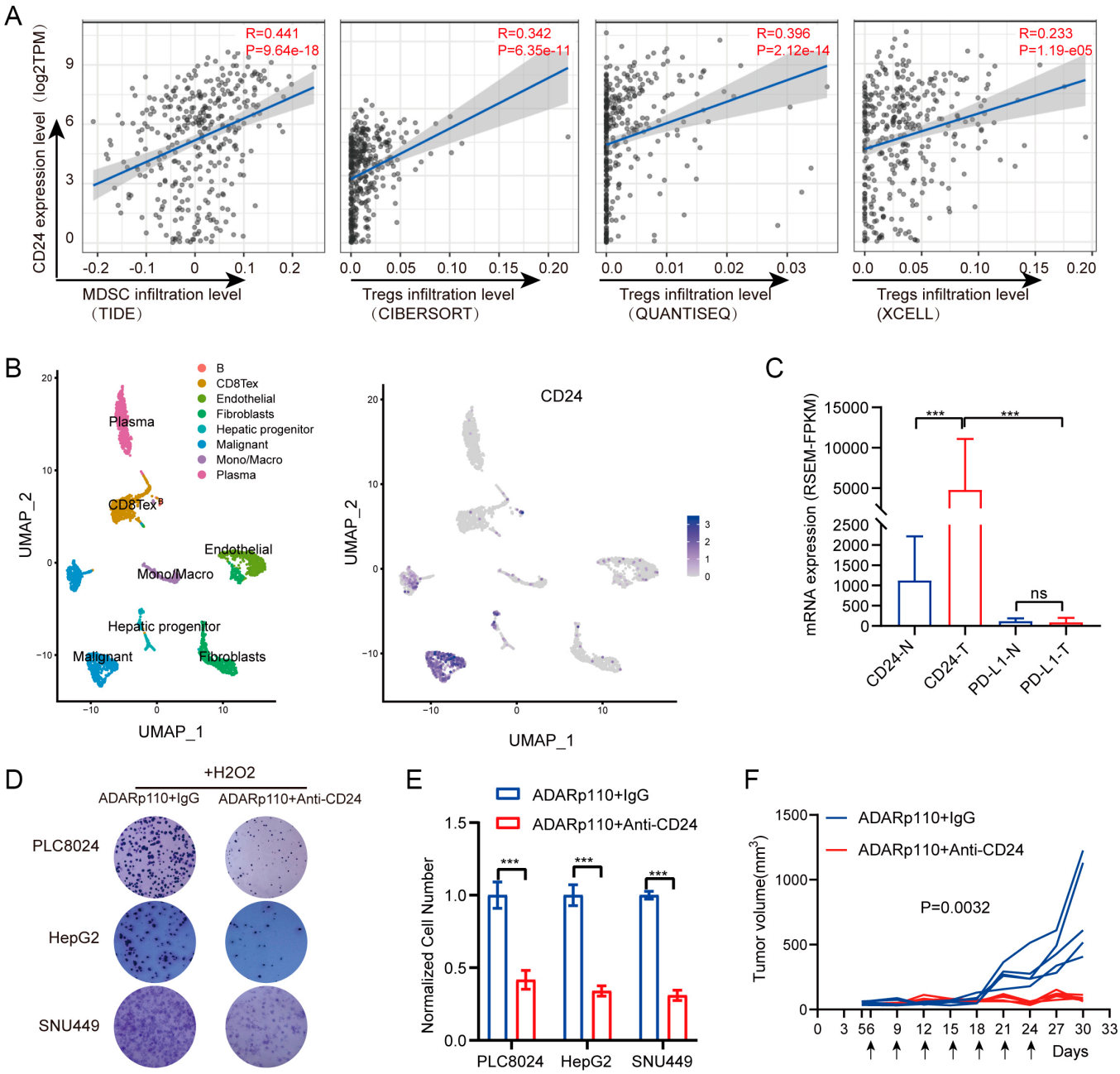

Fig. 7. CD24 as a potential therapeutic target in ADARp110-overexpressed HCC. (*A*) Scatter plot showing the correlation between CD24 expression and the infiltration of MDSCs and Tregs in human HCC, analyzed using the TIMER2.0 platform through indicated computational tools, including CIBERSORT, QUANTISEQ, and XCELL. The *P*-value was calculated using Pearson's correlation coefficient. (*B*) *Left* panel: UMAP plot depicting distinct cell populations identified in scRNA-seq data from HCC patients. *Right* panel: visualization of CD24 gene expression density on UMAP. (*C*) mRNA expression of CD24 and PD-L1 in tumor (T) (n = 369) and nontumor (NT) (n = 50) HCC tissues (TCGA-LIHC Datasets). (*D* and *E*) Representative images of clone formation (*D*) and quantitative results (*E*) after treatment with anti-CD24 mAb under oxidative stress (50 μM H_2O_2) (n = 3). 1,000 cells per well of PLC8024 and SNU449; 500 cells per well of HepG2. (*F*) Tumor growth curves following IgG or anti-CD24 antibody treatment (n = 5), with arrows indicating treatment days. Data are presented as mean ± SD. *P*-values were computed using the unpaired Student's *t* test (*C*, *E*, and *F*). $^{**}P < 0.01$, $^{***}P < 0.001$.

significant reduction in tumor growth following anti-CD24 treatment in breast cancer (22). Furthermore, anti-CD24-CAR (chimeric antigen receptor) T cells and anti-CD24-CAR NK cells have exhibited antitumor effects in pancreatic adenocarcinoma and ovarian cancer (40, 41). It is noteworthy that many HCC patients do not express PD-L1, and there is no discernible difference in PD-L1 expression between tumor and nontumor tissues, which could partly explain the limited clinical responses to PD-L1 treatment in HCC. However, CD24 expression is significantly higher than PD-L1 and is almost exclusively expressed on cancer cells in HCC, minimizing the potential off-target effects associated with anti-CD24 mAb treatment. Taken together, our findings highlight the therapeutic potential of targeting CD24, particularly in HCC cases with high ADARp110 expression.

Materials and Methods

Clinical Samples. Clinical samples were procured from patients who underwent hepatectomy at Sun Yat-sen University Cancer Center (Guangzhou, China). A total of 69 pairs of frozen primary tumor and adjacent nontumor tissues were employed in this study. All patients were granted written informed consent, authorizing the use of their tissues and clinical data for scientific research purposes. The study received approval from the Committee for Ethical Review of Research Involving Human Subjects at Sun Yat-sen University Cancer Center.

Animal Experiments. All animal experiments conducted in this study were subjected to thorough review and approval by the Institutional Animal Care and Use Committee at the Southern University of Science and Technology. Rosa26-CAG-LSL-Adarp110 mice were obtained from Cyagen Biosciences (Guangzhou, China). Albumin-Cre mice and H11-GAG-LSL-Myc mice were purchased from the Shanghai Model Organisms Center, Inc (Shanghai, China). Briefly, the conditional overexpression structures of CAG promoter-loxp-Stop-loxp-Adarp110-polyA and CAG promoter-loxp-Stop-loxp-Myc-polyA were inserted into the Rosa26 locus and H11 locus, respectively.

Statistical Analysis. Statistical analyses were conducted using GraphPad Prism 9.0. To compare the mRNA and protein levels of ADAR1 and CD24 in paired nontumor and tumor samples, a paired two-tailed Student's *t* test was employed. To compare the number of foci, tumor volume, and relative gene expression between two predefined groups, an unpaired two-tailed Student's *t* test was employed. In scenarios where data could be categorized into three or more groups, one-way ANOVA with Duncan's multiple comparisons test was utilized. Kaplan–Meier plots and log-rank tests were used to determine disparities in overall survival. Correlation was examined using Pearson's correlation coefficients analysis. A *P*-value less than 0.05 was considered statistically significant.

Data, Materials, and Software Availability. The publicly accessible databases utilized in this study include The Cancer Genome Atlas Liver Hepatocellular Carcinoma (TCGA-LIHC) dataset (18) and the GSE14520 dataset (23), which has been deposited in the Gene Expression Omnibus (GEO) database (www.ncbi.nlm.nih.gov/geo, accession no. GSE14520). Additionally, public scRNA-seq data were obtained from GSE125449 (42). All other data are included in the article and/or *SI Appendix*.

ACKNOWLEDGMENTS. This research was supported by the Center for Computational Science and Engineering at Southern University of Science and Technology.

Author affiliations: [a]Department of Systems Biology, School of Life Sciences, Southern University of Science and Technology, Shenzhen 518055, China; [b]Department of Clinical Oncology, The University of Hong Kong, Hong Kong 999077, China; [c]State Key Laboratory of Liver Research, The University of Hong Kong, Hong Kong 999077, China; [d]Institute of Cancer Research, Shenzhen Bay Laboratory, Shenzhen 518067, China; [e]Peking University Shenzhen Graduate School, Peking University, Shenzhen 518055, China; [f]Department of Oncology, Xiangyang No.1 People's Hospital, Hubei University of Medicine, Xiangyang 441000, China; [g]Shenzhen Hospital, Southern Medical University, Shenzhen 518000, China; [h]State Key Laboratory of Oncology in Southern China, Sun Yat-Sen University Cancer Center, Guangzhou 510060, China; and [i]Guangdong Provincial Key Laboratory of Tumor Interventional Diagnosis and Treatment, Zhuhai Hospital Affiliated with Jinan University, Zhuhai 519000, China

1. H. Sung *et al.*, Global cancer statistics 2020: GLOBOCAN estimates of incidence and mortality worldwide for 36 cancers in 185 countries. *CA Cancer J. Clin.* **71**, 209–249 (2021).
2. B. Sangro, P. Sarobe, S. Hervás-Stubbs, I. Melero, Advances in immunotherapy for hepatocellular carcinoma. *Nat. Rev. Gastroenterol. Hepatol.* **18**, 525–543 (2021).
3. C. Yang *et al.*, Evolving therapeutic landscape of advanced hepatocellular carcinoma. *Nat. Rev. Gastroenterol. Hepatol.* **20**, 203–222 (2023).
4. A. R. Baker, F. J. Slack, ADAR1 and its implications in cancer development and treatment. *Trends Genet.* **38**, 821–830 (2022).
5. A. Herbert, ADAR and immune silencing in cancer. *Trends Cancer* **5**, 272–282 (2019).
6. B. Song, Y. Shiromoto, M. Minakuchi, K. Nishikura, The role of RNA editing enzyme ADAR1 in human disease. *Wiley Interdiscip Rev. RNA* **13**, e1665 (2022).
7. L. Chen *et al.*, Recoding RNA editing of AZIN1 predisposes to hepatocellular carcinoma. *Nat. Med.* **19**, 209–216 (2013).
8. K. Gumireddy *et al.*, The mRNA-edited form of GABRA3 suppresses GABRA3-mediated Akt activation and breast cancer metastasis. *Nat. Commun.* **7**, 10715 (2016).
9. E. Lazzari *et al.*, Alu-dependent RNA editing of GLI1 promotes malignant regeneration in multiple myeloma. *Nat. Commun.* **8**, 1922 (2017).
10. J. Ramírez-Moya *et al.*, An ADAR1-dependent RNA editing event in the cyclin-dependent kinase CDK13 promotes thyroid cancer hallmarks. *Mol. Cancer* **20**, 115 (2021).
11. V. Tassinari *et al.*, ADAR1 is a new target of METTL3 and plays a pro-oncogenic role in glioblastoma by an editing-independent mechanism. *Genome Biol.* **22**, 51 (2021).
12. L. Qi *et al.*, An RNA editing/dsRNA binding-independent gene regulatory mechanism of ADARs and its clinical implication in cancer. *Nucleic Acids Res.* **45**, 10436–10451 (2017).
13. R. A. Goodman, M. R. Macbeth, P. A. Beal, ADAR proteins: Structure and catalytic mechanism. *Curr. Top Microbiol. Immunol.* **353**, 1–33 (2012).
14. R. Kleinova *et al.*, The ADAR1 editome reveals drivers of editing-specificity for ADAR1-isoforms. *Nucleic Acids Res.* **51**, 4191–4207 (2023).
15. H. Liu *et al.*, Tumor-derived IFN triggers chronic pathway agonism and sensitivity to ADAR loss. *Nat. Med.* **25**, 95–102 (2019).
16. T. Zhang *et al.*, ADAR1 masks the cancer immunotherapeutic promise of ZBP1-driven necroptosis. *Nature* **606**, 594–602 (2022).
17. J. J. Ishizuka *et al.*, Loss of ADAR1 in tumours overcomes resistance to immune checkpoint blockade. *Nature* **565**, 43–48 (2019).
18. J. N. Weinstein *et al.*, Data from "The Cancer Genome Atlas Pan-Cancer analysis project." TCGA-LIHC. https://xenabrowser.net/transcripts/. Deposited 17 October 2013.
19. G. Liu *et al.*, Potential diagnostic and prognostic marker dimethylglycine dehydrogenase (DMGDH) suppresses hepatocellular carcinoma metastasis in vitro and in vivo. *Oncotarget* **7**, 32607–32616 (2016).
20. S. Roessler *et al.*, A unique metastasis gene signature enables prediction of tumor relapse in early-stage hepatocellular carcinoma patients. *Cancer Res.* **70**, 10202–10212 (2010).
21. H. J. Hartwell, K. Y. Petrosky, J. G. Fox, N. D. Horseman, A. B. Rogers, Prolactin prevents hepatocellular carcinoma by restricting innate immune activation of c-Myc in mice. *Proc. Natl. Acad. Sci. U.S.A.* **111**, 11455–11460 (2014).
22. A. A. Barkal *et al.*, CD24 signalling through macrophage Siglec-10 is a target for cancer immunotherapy. *Nature* **572**, 392–396 (2019).
23. S. Roessler *et al.*, Data from "A unique metastasis gene signature enables prediction of tumor relapse in early-stage hepatocellular carcinoma patients". NCBI GEO. https://www.ncbi.nlm.nih.gov/geo/query/acc.cgi?acc=gse14520. Deposited 1 December 2010.
24. C. X. George, C. E. Samuel, Human RNA-specific adenosine deaminase ADAR1 transcripts possess alternative exon 1 structures that initiate from different promoters, one constitutively active and the other interferon inducible. *Proc. Natl. Acad. Sci. U.S.A.* **96**, 4621–4626 (1999).
25. A. J. Ozga, M. T. Chow, A. D. Luster, Chemokines and the immune response to cancer. *Immunity* **54**, 859–874 (2021).
26. S. G. Moreno, Depleting Macrophages In Vivo with Clodronate-Liposomes. *Methods Mol. Biol.* **1784**, 259–262 (2018).
27. O. Solomon *et al.*, RNA editing by ADAR1 leads to context-dependent transcriptome-wide changes in RNA secondary structure. *Nat. Commun.* **8**, 1440 (2017).
28. D. Szklarczyk *et al.*, The STRING database in 2023: Protein-protein association networks and functional enrichment analyses for any sequenced genome of interest. *Nucleic Acids Res.* **51**, D638–d646 (2023).
29. L. Ma *et al.*, Tumor cell biodiversity drives microenvironmental reprogramming in liver cancer. *Cancer Cell* **36**, 418–430.e416 (2019).
30. G. Wang *et al.*, ADAR1 prevents liver injury from inflammation and suppresses interferon production in hepatocytes. *Am. J. Pathol.* **185**, 3224–3237 (2015).
31. R. Chen, C. A. Ishak, D. D. De Carvalho, Endogenous retroelements and the viral mimicry response in cancer therapy and cellular homeostasis. *Cancer Discov.* **11**, 2707–2725 (2021).
32. K. A. Lawson *et al.*, Functional genomic landscape of cancer-intrinsic evasion of killing by T cells. *Nature* **586**, 120–126 (2020).
33. M. J. Pittet, O. Michielin, D. Migliorini, Clinical relevance of tumour-associated macrophages. *Nat. Rev. Clin. Oncol.* **19**, 402–421 (2022).
34. I. X. Wang *et al.*, ADAR regulates RNA editing, transcript stability, and gene expression. *Cell Rep.* **5**, 849–860 (2013).
35. M. Sakurai *et al.*, ADAR1 controls apoptosis of stressed cells by inhibiting Staufen1-mediated mRNA decay. *Nat. Struct. Mol. Biol.* **24**, 534–543 (2017).
36. X. Wang, L. Vukovic, H. R. Koh, K. Schulten, S. Myong, Dynamic profiling of double-stranded RNA binding proteins. *Nucleic Acids Res.* **43**, 7566–7576 (2015).
37. N. Fujikuni *et al.*, Hypoxia-mediated CD24 expression is correlated with gastric cancer aggressiveness by promoting cell migration and invasion. *Cancer Sci.* **105**, 1411–1420 (2014).
38. Y. Tolkach *et al.*, DNA promoter methylation and ERG regulate the expression of CD24 in prostate cancer. *Am. J. Pathol.* **191**, 618–630 (2021).
39. J. Vegfors, S. Petersson, A. Kovács, K. Polyak, C. Enerbäck, The expression of Psoriasin (S100A7) and CD24 is linked and related to the differentiation of mammary epithelial cells. *PLoS One* **7**, e53119 (2012).
40. R. Klapdor *et al.*, Characterization of a novel third-generation anti-CD24-CAR against ovarian cancer. *Int. J. Mol. Sci.* **20**, 660 (2019).
41. A. Maliar *et al.*, Redirected T cells that target pancreatic adenocarcinoma antigens eliminate tumors and metastases in mice. *Gastroenterology* **143**, 1375–1384.e75 (2012).
42. L. Ma *et al.*, Data from "Tumor cell biodiversity drives microenvironmental reprogramming in liver cancer". NCBI GEO. https://www.ncbi.nlm.nih.gov/geo/query/acc.cgi?acc=GSE125449. Deposited 6 October 2019.